Optical and Electrical Properties of Amorphous Carbon Thin Films Grown from Mushroom Waste Oil using Chemical Vapor Deposition (CVD)

Amirah Radhianie-Rining[1], Nurfadzilah Ahmad[1]*, Firdaus Muhammad-Sukki[2], Wan Abd Al Qadr Imad Wan-Mohtar[3]

[1]Solar Research Institute (SRI), Universiti Teknologi MARA, 40450 Shah Alam, Selangor, Malaysia
[2]School of Computing, Engineering & Built Environment, Merchiston Campus, Edinburgh Napier University, Edinburgh EH10 5DT, UK
[3]Functional Omics and Bioprocess Development Laboratory, Institute of Biological Sciences, Faculty of Science, Universiti Malaya, 50603 Kuala Lumpur, Malaysia

*Corresponding author : nurfadzilah6344@uitm.edu.my

ABSTRACT

Amorphous carbon thin films have been successfully deposited using the Chemical Vapor Deposition (CVD) technique with various amounts of natural oyster mushroom (*P.ostreatus*) waste oil as carbon precursors onto the glass substrates. This study examined the impact of varying precursor amounts on the assessment of the properties of amorphous carbon thin films, especially the optical and electrical characteristics. The lower part of the oyster mushroom, which is normally discarded, was harvested and extracted into mushroom waste oil using Soxhlet extraction. CVD technique was used for the deposition of amorphous carbon, where mushroom waste oil was used as a precursor and glass as a substrate. Then, UV-Vis spectroscopy, current-voltage (I-V) measurement, and Raman spectroscopy were utilized for characterization. The findings demonstrate that the thin films show a combination of sp^3 and sp^2 bonded carbon atoms, which is common for amorphous carbon. The lowest optical band gap, 0.37 eV, and the highest electrical conductivity, 1.51×10^{-5} $S.cm^{-1}$ was deposited at 2 ml of oyster mushroom waste oil. These results indicate that amorphous carbon grown from mushroom waste oil is capable of being a 'green' alternative as a source for carbon-based solar cells in the future.

KEYWORDS: Amorphous carbon, Chemical Vapor Deposition, Natural oil precursor, Mushroom waste oil

Received 20 January 2025; Revised 21 February 2025; Accepted 10 April 2025
Doi: https://doi.org/10.59953/paperasia.v41i3b.414

1. INTRODUCTION

Carbon-based materials have gained the researchers' attention due to their propensity to yield a wide variety of allotropes such as amorphous, diamond, graphene, and graphite (Saputri et al., 2020; Kim et al., 2021; Kothandam et al., 2023; Dhameliya et al., 2024;). Different types of carbon allotropes can be distinguished based on the type of chemical bond and hybridization. Diamond-like carbon (DLC), which contains 100% sp^3 hybridization makes it an insulator, whereas 100% sp^2 hybridization in graphite makes it a great conductor. Meanwhile, mixed sp^2 and sp^3 hybridization is present in amorphous carbon (Priyanto et al., 2024).

The unique properties of amorphous carbon (a-C) make them useful in various fields. These qualities include low cost, high hardness, high chemical inertness, ease of production, high optical transmittance, low coefficient friction and an optical band gap that can be tuned (Cui et al., 2012; Zhang et al., 2022a; Kang et al., 2023; Roy et al., 2023) By merely changing the ratio of its sp^3 and sp^2, their electrical, mechanical, optical, and structural properties are affected (Chen et al., 2015). The hydrogen content, the deposition parameter, and the carbon precursor are said to influence the percentage of carbon hybridization. Hydrocarbon compounds can be used as the carbon precursor in Chemical Vapor Deposition (CVD), which is one of the many techniques for creating a-C thin films (Priyanto et al., 2024).

Several carbon sources from renewable and non-renewable origins have been identified to be capable of creating allotrope carbon, including methane, acetylene, ethanol, and ethylene, as well as from renewable precursors like camphor oil, palm oil, palmyra sugar, etc. (Ishak et al., 2015; Priyanto et al., 2024). The common factor among these sources is that they are chosen as they are hydrocarbon precursors, which are mainly made up of carbon, hydrogen, and oxygen molecules. Most of the carbonaceous compounds employed in the early phases of discovering the right precursors have negative effects on the environment and human health, as they are toxic and explosives (Yan et al., 2020; Ouyang et al., 2021). Besides those precursors, oyster mushroom (*P. ostreatus*) waste oil has the potential to synthesize a-C thin films as they are ecologically friendly precursors.

Pleurotus ostreatus, also known as oyster mushrooms, are edible mushrooms with unique flavors and medicinal benefits. Together with button and shiitake mushrooms (*Agaricus bisporus* and *Lentinula edodes*), which account for 16% of the world's supply, oyster mushrooms are also among the most farmed and consumed in the world (Zhou et al., 2023). *Pleurotus ostreatus*'s bioactive significance and other health-promoting qualities have garnered a lot of attention. For example, this edible mushroom has a high content of proteins, phenolics, flavonoids, glycoproteins, terpenoids, steroids, and alkaloids. It also has pharmacological and therapeutic properties that include anti-inflammatory, anti-diabetic, anti-viral, anti-cancer, anti-tumor, antioxidant, and antihypertensive properties (Elhusseiny et al., 2021; Ianni et al., 2021). To meet the objective of selecting the precursors that are low cost, high in carbon content, abundant, and environmentally friendly, the oyster mushroom waste oil was chosen due to the mentioned benefits.

CVD has been used to successfully produce a-C thin films from biomass sources. CVD is the best technique for deposition on large substrates and complex structures, resulting in inexpensive manufacturing. This method has been widely used in the industry, especially for semiconductors as they can synthesize high performance and quality a-C. This method is also frequently mentioned in the previous study (Kamaruzaman et al., 2020). These films, which are made from palm sugar, palm oil, and camphor oil, have been effectively applied to glass for a variety of uses, most notably solar cells. Kamaruzaman et al. (2020), for example, used this method to successfully deposit undoped and iodine-doped a-C (a-C:I) thin films from camphor oil, revealing that iodine doping could improve the electrical properties. Ishak et al. (2015) reported that boron-doped and undoped a-C thin films were successfully produced using the CVD method for solar cell applications, with respective efficiencies of 1.543% and 0.1302%. This was achieved through the use of natural palm oil as a carbon precursor. Aerosol-assisted CVD (AACVD) has been successfully used by Fadzilah et al. (2014a) to deposit nitrogen-doped a-C thin films from camphor oil for solar cell applications. The efficiency of AACVD is 0.001648% at a deposition temperature of 650 °C. So far, a-C thin films using mushrooms as carbon precursors have not yet been developed (Fadzilah et al., 2014a).

This paper reports the synthesis of a-C thin film using oyster mushroom waste oil, a novel alternative "green" carbon precursor not previously used by researchers. Using oyster mushroom waste oil as a carbon source, these a-C thin films were successfully deposited on glass substrates through the CVD method. The purpose of this work was to examine how the various concentrations of mushroom waste oil affected the structural, optical, and electrical characteristics.

2. METHODOLOGY

2.1 Oyster Mushroom (*P. ostreatus*) Waste Oil Preparation

The lower part of the stem of an oyster mushroom, which is commonly discarded, was cut off from its fruiting body during the oyster mushroom harvest in the Mushrooms Unit, Agrotechnology Section, Universiti Putra Malaysia (UPM). The waste mushroom biomass (WMB) was cleaned off the soil and insects and dried at 50 °C for 24 h using an oven dryer. The dried WMBs were then ground to a fine powder using the laboratory blender. The floured WMB (FWMB) was stored in a bottle, along with silica gel to keep it dry until use.

Using Soxhlet extraction, the extraction of oils from mushroom waste was conducted with hexane as solvent. 40 g of FWMB was placed in a thimble with 400 ml of hexane and heated at 80 °C for 4 h. After extraction, the oils from WMB were collected and evaporated to remove the solvent using a rotary evaporator at 50 °C. The extracted oils were dried further at room temperature under a laminar flow hood to ensure all of the hexane was removed. The dried oils were then re-dissolved in hexane and stored at room temperature until further analyses.

2.2 Deposition of Amorphous Carbon (a-C) Thin Films

Chemical vapor deposition (CVD) was utilized in the deposition of amorphous carbon thin films. The CVD system which is a double furnace setup, consists of a heater, a tube made of quartz, and a water bubbling system. To produce a-C thin films, WMB oil was utilized as the carbon precursor, while argon gas was employed as a carrier gas. An alumina boat containing various amounts of WMB oil, 1-4 ml, was put in the first furnace, which heated to 350 °C inside a quartz tube. Then, the second furnace was used to heat an alumina boat containing a 2 cm x 2 cm glass substrate to 550 °C. The argon gas was kept flowing through a quartz tube with a flow rate of 45 standard cubic centimeters per minute (sccm). For 30 mins, the depositions were done using a variety of precursor amounts. After 30 mins, the samples were cooled down until both furnaces reached room temperature before being brought out of the quartz tube. Following that, for the optical and structural characteristics, Raman Spectroscopy, surface profiler and UV-Vis Spectroscopy were used to characterize the samples. Meanwhile, for the electrical characteristic, current-voltage (I-V) measurements were used. Gold was deposited on the samples using a thermal evaporator in order to assess the electrical properties of a-C thin films for the I-V measurement.

3. RESULTS AND DISCUSSION

3.1 Raman Spectroscopy

Raman spectroscopy was utilized to investigate the structural properties of a-C due to its ability to examine the behavior of bonding, internal stress, etc., in a-C thin films in a fast and non-destructive way (Kamaruzaman et al., 2012; Mohagheghpour et al., 2016; Dychalska et al., 2019; Orlando et al., 2021). The Raman spectrum of the deposition of a-C thin films at various amounts of oyster mushroom waste oil in the 1000-2000 cm^{-1} range are displayed in **Figure 1**.

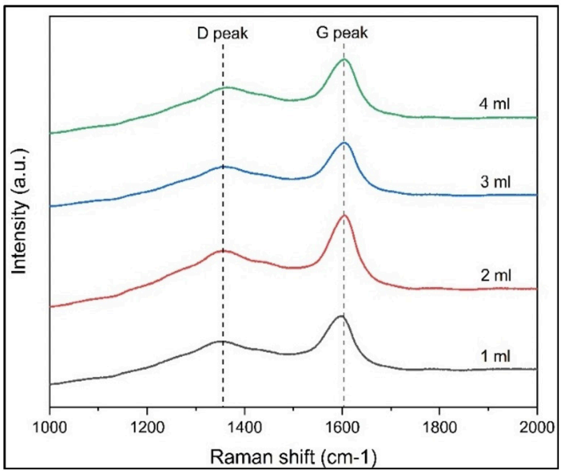

Figure 1: *Raman spectrum of the a-C*

From the Raman spectrum, it is likely that the a-C thin films are an amorphous carbon due to the absence of 2D Raman peaks (Mitra et al., 2024). The D peak and G peak, which shows the coexistence of sp^2 and sp^3 bonding, are the two peaks that are present in a typical amorphous carbon. In general, the D peak indicates the disordered or defective carbon that is related to the presence of the edges and grains of the carbon, which means that the existence of this peak is not possible in perfect graphite. Meanwhile, the G peak corresponds to the presence of π electron delocalization or sp^2 clustering in the samples as it appears from all of the sp^2 sites. This is because of its involvement in the stretching movement of the carbon pair sp^2 atoms (Fadzilah et al., 2013; Chen et al., 2015; Gabhi et al., 2020; Moseenkov et al., 2023). Thus, due to this, the low value of the intensity ratio (I_D/I_G) shows that the sp^3 content is higher. Then, the high value of I_D/I_G ratio indicates the clustering and ordering of the sp^2 content for a-C (Dychalska et al., 2019). For a simple additional explanation about the Raman spectra peaks for amorphous carbon, Moseenkov et al. (2023) have provided a detailed analysis of the characteristics of several modes that can be found in amorphous carbon. The D peak (D_2 mode), which is only present in disordered carbon structures and not in perfect graphite, is considered to have existed due to the vibration of the A_{1g} symmetry and is situated at 1310 to 1390 cm^{-1}. The G peak, which is present because of the in-plane graphitic vibrations with the E_{2g} symmetry is situated from 1575 to 1600 cm^{-1}. In addition, there is also a D_3' mode that is situated at 1450 to 1490 cm^{-1} and D_3" mode located at 1520 to 1555 cm^{-1}) which both modes are linked with the existence of a-C and D_4 mode at 1615 to 1650 cm^{-1} which vibrates similarly to the G peak.

In this study, the approximate positions of D and G peaks were found at ~1350 and ~1600 cm^{-1}, respectively, which are typical for a-C. However, the results show that the G peaks for 2 ml, 3 ml, and 4 ml precursors were shifted slightly above 1600 cm^{-1} that is beyond the usual range of G peaks. It likely occurred because of the increase of the compressive stress with the increase of the thickness during deposition which results in the upward shift of the G-peak position (Mohagheghpour et al., 2016). The Raman intensity ratio (I_D/I_G) for a-C thin films was calculated from the Raman peak position, as indicated in **Table 1** and **Figure 2**. The intensity ratio is calculated to study the change in the carbon bonding structure of the film which implements that the I_D/I_G ratio indicates the content of sp^2 and sp^3 in the a-C (Crespi et al., 2020; Zhang et al., 2022b). In **Table 1**, the findings revealed that when the amount of oyster mushroom waste oil (precursor) increases, the I_D/I_G ratio shows a slight decrease from 0.72 to 0.70. This proves that the low I_D/I_G ratio values of the samples indicate the increase in the crystallinity behavior of a-C while the high I_D/I_G ratio demonstrates the graphitization of the film structure because of the change in the sp^2 bonds (Fadzilah et al., 2014b; Ono et al., 2024).

Table 1: *The D peak and G peak position, and the ratio of intensity of a-C*

Amount precursor (ml)	D peak position (cm^{-1})	G peak position (cm^{-1})	Intensity ratio (I_D/I_G)
1	1345	1595	0.72
2	1356	1603	0.71
3	1359	1604	0.70
4	1361	1603	0.70

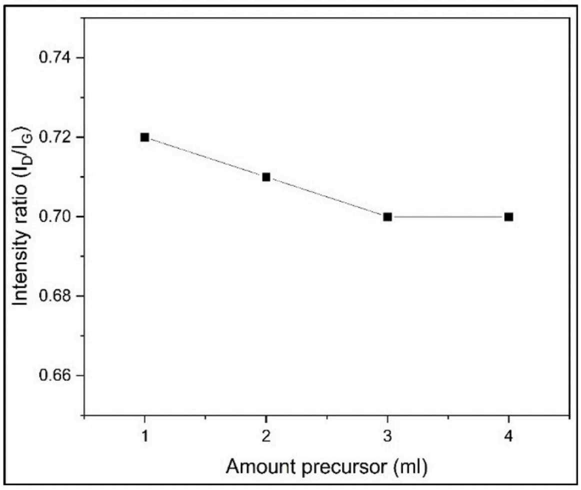

Figure 2: *The intensity ratio of the a-C*

3.2 UV-Vis Spectroscopy

The optical characteristics of the a-C thin films (e.g. optical transmittance and band gap) were investigated using UV-Vis Spectroscopy, while a surface profiler was used to obtain the average thickness of the samples. In this study, the wavelength of the spectroscopy used ranged from 300 nm to 800 nm. The graph of optical transmittance against the wavelength of the a-C thin films is displayed in **Figure 3**. In the visible range (390-790 nm), the optical transmittance that was found has a value that is higher than 80%. As the optical transmittance is strongly dependent on the thickness of the a-C thin films, it can be seen in this research that the percentage of the optical transmittance decreases as the thickness of the films increases due to the increasing amount of the precursor (Mohagheghpour et al., 2016). When the films are thicker, they appear less transparent compared to the thinner films. **Table 2** shows that the highest spectrum of optical transmittance (89.95%) has the thinnest a-C thin films (92 nm) when deposited at 1 ml precursor, while the films with the thickest films (313 nm) that were deposited at 4 ml precursor show the lowest transmittance (80.81%) spectrum.

Eq. (1) illustrates the application of the Tauc relationship to determine the optical band gap of a-C thin films

$$(\alpha h\nu)^{1/2} = B(E_g - h\nu) \qquad (1)$$

The optical band gap (E_g) can be defined as the energy differential between a material's valence and conduction bands. It is reported that the band gap has a relationship with the sp^3 and sp^2 bonds ratio in the films (Crespi et al., 2020). Using the Tauc relation, the linear portion of the curve at a = 0 was extrapolated to yield the a-C thin films E_g. The graph of the Tauc plot of $(\alpha h\nu)^{1/2}$ for a-C thin films against photon energy at varying amounts of oyster mushroom waste oil is displayed in **Figure 4**. According to Li et al. (2018), the optical properties associated with the coexistence and relative ratio of the carbon sites of sp^3 and sp^2, where the increasing sp^2 content causes the optical band gap to narrow, are said to be related (Li et al., 2018).

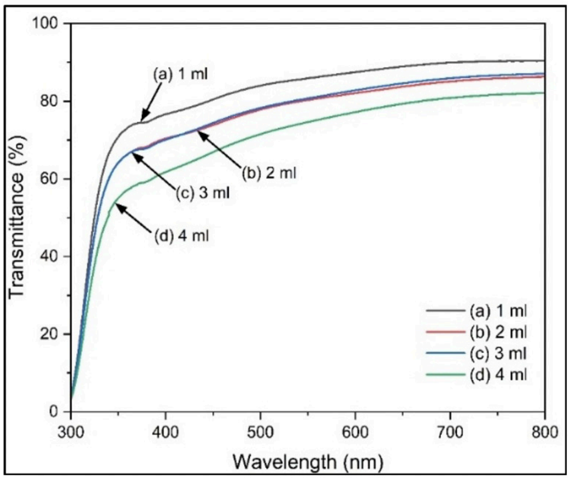

Figure 3: *The graph of optical transmittance against wavelength of a-C thin films*

Table 2: *The highest transmittance and optical band gap a-C*

Amount precursor (ml)	Highest transmittance (%)	Optical band gap, (eV)	Average thickness (nm)
1	89.95	0.80	92
2	85.07	0.37	115
3	85.90	0.57	226
4	80.81	0.65	313

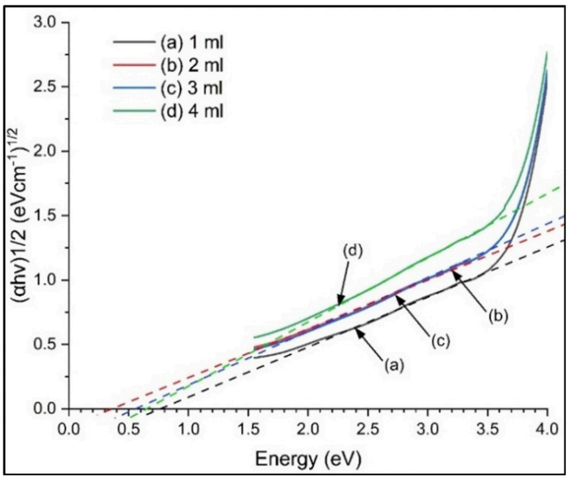

Figure 4: *The graph of Tauc plot of against photon energy for a-C thin films*

From **Table 2**, the E_g for a-C thin films when deposited at 1 ml of the precursor was 0.80 eV which then decreased to 0.37 eV at 2 ml precursor and progressively increased to 0.57 eV and 0.65 eV, as the amount of precursor increased to 3 ml and 4 ml, respectively. Here, the samples with higher optical band gaps can be considered as having smaller sp^2 cluster while the lower band gaps indicate a larger size of sp^2 cluster. This is due to the fact that the sizes of the conjugated p_z electron network or more precisely the sp^2 bonded carbon dictates the characteristics of the band gap (Baule et al., 2024).

The mechanical, optical, chemical, and electrical properties of a-C thin films are determined by an amorphous network that is mostly composed of sp^3 and sp^2 carbon-carbon bonds, which in contrast to the sp^3 hybridized crystalline diamond. Both π and σ bonds exist in sp^2 carbon, but the delocalized π electrons that occupy the p_z orbital is the cause of the electrical conductivity. In non-doping circumstances, the electrons are firmly bound together by the four σ bonds in sp^3 bonded carbon, which results in dielectric characteristics. Insufficient electrical conductivity resulted from the isolation of the sp^2 sites at low sp^2 carbon concentrations, where only a few electrons can be conjugated. Therefore, conjugated p_z electrons are produced as the total sp^2 increases, which results in the increase of sp^2 cluster sizes as well (Baule et al., 2024).

In this study, we notice that the optical band gap increases with the percentage of optical transmittance. However, we have to consider the thickness of the samples since, as mentioned before, the transmittance is affected by the film thickness which is increasing by the rising amount of precursor (Mohagheghpour et al., 2016). For instance, **Table 2** shows that the 1 ml precursor sample is the thinnest (92 nm) of all the samples, but it has the widest band gap (0.80 eV) and the highest percentage of optical transmittance (89.95%). In contrast, for sample 2 ml precursor, as the thickness of the a-C thin films increased (to 115 nm), the optical band gap (0.37 eV) and the percentage of transmittance (85.07%) declined. The increase in sp^2 in the films, which would also influence the conductivity, may be the cause of the decreasing trend of the band gap (Kamaruzaman et al., 2020). However, the optical band gap increases gradually to 0.57 eV (3 ml) and 0.65 eV (4 ml) after 2 ml of precursor. This increase in thickness is probably caused by the absorption of the film thickness (Astinchap & Laelabadi, 2019).

3.3 Current-Voltage (I-V) Measurement

For the current-voltage (I-V) measurement, 2-point probe was used to characterize the electrical characteristics of a-C thin film. To achieve the ohmic contacts, the thermal evaporator deposited 60 nm of 99.9% gold (Au) on top of the film. The conductivity, a, and resistivity, ρ were calculated using Eq. (2) and Eq. (3) (Robaiah et al., 2023)

$$\rho = \left(\frac{V}{I}\right)\left(\frac{wt}{L}\right) \quad \text{in unit } \Omega.\text{cm} \qquad (2)$$

$$\sigma = \frac{1}{\rho} \quad \text{in unit S.cm}^{-1} \qquad (3)$$

Generally speaking, there are both sp^3 and sp^2 carbon atoms in varying amounts for a-C. Whereas ordered sp^3 carbons, like diamonds, are insulators, ordered sp^2 carbons, like graphene, carbon nanotubes, and graphite, are conductors. Thus, the conduction of electricity is caused by the π electrons in the sp^2 carbons (Gabhi et al., 2020). The current-voltage (I-V) characteristic curve of a-C thin films is displayed in **Figure 5**. It is evident that the results were linear which indicates that the current progressively increased as the voltage increased at room temperature. A higher slope denotes a lower resistance value (Kamaruzaman et al., 2020).

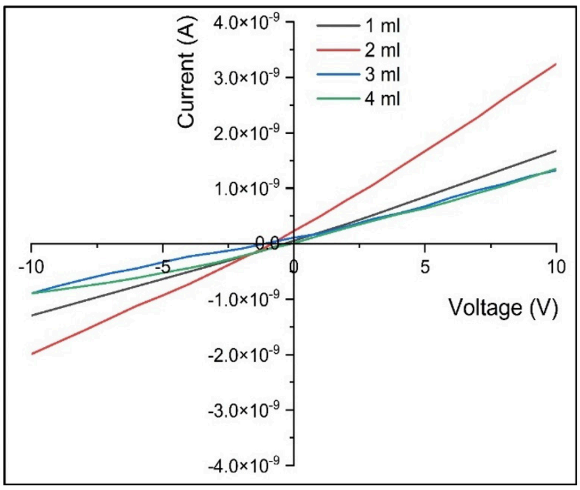

Figure 5: *The I-V characteristic curve of a-C thin films*

The electrical conductivity of a-C thin films against the quantity of precursor is shown in **Table 3** and **Figure 6(a)**. The conductivity was found to be increased from 1.08×10^{-5} S.cm^{-1} to 1.51×10^{-5} S.cm^{-1} at 1 ml to 2 ml and then significantly declined to 3.18×10^{-6} S.cm^{-1} at 3 ml then continuing to decrease to 2.44×10^{-6} S.cm^{-1} at 4 ml. **Table 3** and **Figure 6(b)** show that the resistivity decreased from 9.29×10^4 Ω.cm to 6.61×10^4 Ω.cm at 1 ml to 2 ml and increased to 3.15×10^5 Ω.cm and continue increasing 4.10×10^5 Ω.cm at 4 ml. Accordingly, the results demonstrate that an increase in sp^3 concentration occurs when the conductivity falls and the resistivity rises (Kamaruzaman et al., 2012). In addition to sp^2 cluster size, carrier mobility, and density also affect the electrical conductivity. The quantity of π states of sp^2 sites may decrease as the compressive stress rises with the increasing film thickness. Furthermore, the decrease in the band gap results in an increase in electrical conductivity. Consequently, a decrease in the band gap and an increase in the number of π states per cluster during deposition are the causes of the decrease in resistivity (Mohagheghpour et al., 2016). Since the electrical conductivity at 2 ml was the highest, we can clarify that 2 ml is the optimum amount of oyster mushroom waste oil to produce a-C thin films.

Table 3: *The resistivity and electrical conductivity of a-C thin films deposited at various amounts of oyster mushroom waste oil using CVD*

Amount precursor (ml)	Resistivity (Ω.cm)	Conductivity (S.cm^{-1})
1	9.29×10^4	1.08×10^{-5}
2	6.61×10^4	1.51×10^{-5}
3	3.15×10^5	3.18×10^{-6}
4	4.10×10^5	2.44×10^{-6}

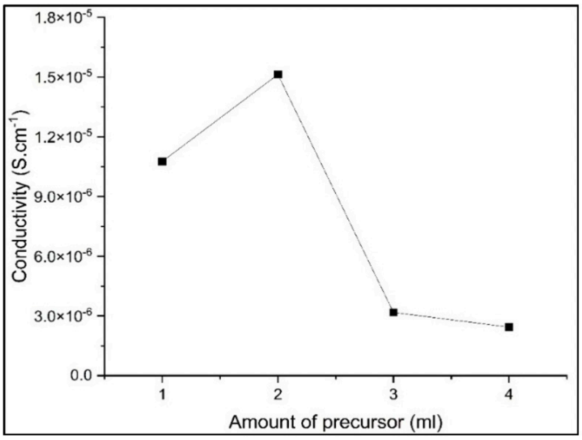

(a)

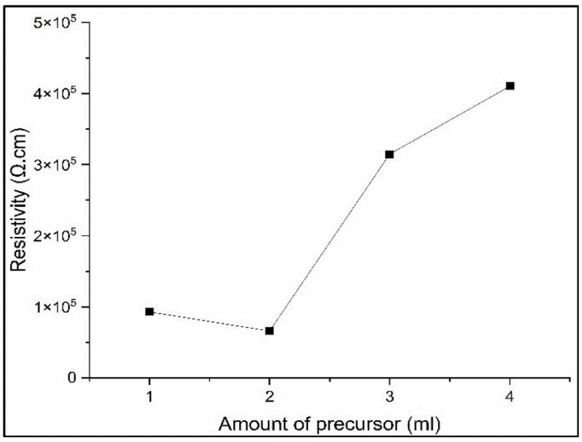

(b)

Figure 6: *a) Electrical conductivity b) Resistivity of a-C thin films*

4. CONCLUSION

In conclusion, the a-C thin films were produced by the CVD method from oyster mushroom waste oil as a natural carbon precursor, which has not yet been investigated by previous researchers. Raman spectroscopy can be used to confirm the characteristics of amorphous carbon with the presence of the D peak and G peak in the a-C thin films. It was discovered that 2 ml of oyster mushroom waste oil could form a-C thin films with higher sp^2 carbon content as the intensity (I_D/I_G) ratio is high. Using UV-Vis Spectroscopy, the optical properties were examined. At 2 ml of oyster mushroom waste oil, the lowest optical band gap was measured at 0.37 eV, indicating a larger size of sp^2 cluster. The electrical properties of the a-C thin films were investigated using the current-voltage (I-V) measurement. It was found that when deposited at 2 ml of precursor, their electrical conductivity is the highest at 1.51×10^{-5} S.cm^{-1} and their resistivity is the lowest at 6.61×10^4 Ω.cm. The electrical conductivity can be seen to increase due to the decrease in the band gap and the increase of the π states per sp^2 cluster. These could serve as the basis for future studies on the synthesis and optimization parameters of a-C thin films using oyster mushroom waste oil as a carbon precursor for advancement. Being a renewable, 'green', and inexpensive source, it has the capability to be a source for carbon-based solar cell applications in the future.

ACKNOWLEDGEMENT

The authors would like to thank the Research Management Institute (RMI) of Universiti Teknologi MARA (UiTM) and the Ministry of Higher Education of Malaysia (MOHE) for the funding. This research was supported by Grant No. FRGS/1/2021/TK0/UITM/02/12 under MOHE. The author would also like to thank the staff of the Nano-Electronic Centre (NET) of UiTM for the instrument and facilities

REFERENCES

Astinchap, B., & Laelabadi, K. G. (2019). Effects of substrate temperature and precursor amount on optical properties and microstructure of CVD deposited amorphous TiO2 thin films. *Journal of Physics and Chemistry of Solids, 129*, 217-226. https://doi.org/10.1016/j.jpcs.2019.01.012

Baule, N., Tsu, D. V., Haubold, L., & Schuelke, T. (2024). The inner workings of sp2 clusters in nitrogen-incorporated tetrahedral amorphous carbon thin films according to optical analyses. *Diamond and Related Materials, 145*, 111111. https://doi.org/10.1016/j.diamond.2024.111111

Chen, T.-S., Hsueh, Y.-C., Chiou, S.-E., & Shiue, S.-T. (2015). The effect of the native silicon dioxide interfacial layer on photovoltaic characteristics of gold/p-type amorphous boron carbon thin film alloy/

silicon dioxide/n-type silicon/aluminum solar cells. *Solar Energy Materials and Solar Cells, 137*, 185-192. https://doi.org/10.1016/j.solmat.2015.02.002

Crespi, Â. E., Ballage, C., Hugon, M. C., Robert, J., Lundin, D., Vickridge, I., Alvarez, J., & Minea, T. (2020). Low resistivity amorphous carbon-based thin films employed as anti-reflective coatings on copper. *Thin Solid Films, 712*, 138319. https://doi.org/10.1016/j.tsf.2020.138319

Cui, T., Lv, R., Huang, Z.-H., Zhu, H., Jia, Y., Chen, S., Wang, K., Wu, D., & Kang, F. (2012). Low-temperature synthesis of multilayer graphene/amorphous carbon hybrid films and their potential application in solar cells. *Nanoscale Research Letters, 7*, 1-7. https://doi.org/10.1186/1556-276X-7-453

Dhameliya, T. M., Bharadia, H. A., Shah, J. K., Sureja, D. K., & Bodiwala, K. B. (2024). Future of environment with carbon allotropes. *Nirma University Journal of Pharmaceutical Sciences, 11*(1), 33-54.

Dychalska, A., Fabisiak, K., Paprocki, K., Koczorowski, W., Trzcinski, M., & Szybowicz, M. (2019). The effect of low temperature thermal treatment on structural and chemical composition of a-C film with nc-G admixture studied by Raman spectroscopy. *Diamond and Related Materials, 95*, 44-54. https://doi.org/10.1016/j.diamond.2019.03.016

Elhusseiny, S. M., El-Mahdy, T. S., Awad, M. F., Elleboudy, N. S., Farag, M. M. S., Yassein, M. A., & Aboshanab, K. M. (2021). Proteome Analysis and In Vitro Antiviral, Anticancer and Antioxidant Capacities of the Aqueous Extracts of Lentinula edodes and Pleurotus ostreatus Edible Mushrooms. *Molecules, 26*(15). https://doi.org/10.3390/molecules26154623

Fadzilah, A., Dayana, K., & Rusop, M. (2013). Fabrication and characterization of camphor-based amorphous carbon thin films. *Procedia Engineering, 56*, 743-749. https://doi.org/10.1016/j.proeng.2013.03.188

Fadzilah, A., Kamaruzaman, D., Siran, Y. M., Rejab, S. A. M., Asis, A. J., Tahirruddin, S., & Mahmood, M. R. (2014a). Nitrogen Doping of Amorphous Carbon by Aerosol-Assisted Chemical Vapor Deposition for Carbon-Based Solar Cell Applications. *Advanced Materials Research, 832*, 706-711.

Fadzilah, A., Kamaruzaman, D., Siran, Y. M., Syahril Anuar, M. R., Asis, A. J., Syawaluddin, T., & Mahmood, M. R. (2014b). Influence of Deposition Time on Amorphous Carbon Thin Films Performance with Aerosol-Assisted Chemical Vapor Deposition. *Advanced Materials Research, 832*, 712-717.

Gabhi, R., Basile, L., Kirk, D. W., Giorcelli, M., Tagliaferro, A., & Jia, C. Q. (2020). Electrical conductivity of wood biochar monoliths and its dependence on pyrolysis temperature. *Biochar, 2*, 369-378. https://doi.org/10.1007/s42773-020-00056-0

Ianni, F., Blasi, F., Angelini, P., Simone, S. C. D., Angeles Flores, G., Cossignani, L., & Venanzoni, R. (2021). Extraction Optimization by Experimental Design of Bioactives from Pleurotus ostreatus and Evaluation of Antioxidant and Antimicrobial Activities. *Processes, 9*(5), 743.

Ishak, A., Dayana, K., Mamat, M., Malek, M., & Rusop, M. (2015). Nano-structured amorphous carbon films using novel palm oil precursor for solar cell applications. *Optik, 126*(18), 1610-1612. https://doi.org/10.1016/j.ijleo.2015.05.030

Kamaruzaman, D., Fadzilah, A., & Rusop, M. (2012). The Effect of Camphor Oil Amounts on the Properties of Amorphous Carbon Thin Films by Thermal Chemical Vapor Deposition. *Advanced Materials Research, 576*, 611-614.

Kamaruzaman, D., Rosly, M. A., Annuar, I., Ahmad, N., & Mahmood, M. R. (2020, April). Deposition and characterization of amorphous carbon thin film by thermal CVD. In *Journal of Physics: Conference Series* (Vol. 1529, No. 2, p. 022049). IOP Publishing.

Kang, J., Yang, X., Hu, Q., Cai, Z., Liu, L.-M., & Guo, L. (2023). Recent Progress of Amorphous Nanomaterials. *Chemical Reviews, 123*(13), 8859-8941. https://doi.org/10.1021/acs.chemrev.3c00229

Kim, J.-H., Kim, H.-G., & Kwac, L.-K. (2021). High-efficient Schottky-junction silicon solar cell using silver nanowires covering nitrogen-doped amorphous carbon. *Current Applied Physics, 26*, 1-8. https://doi.org/10.1016/j.cap.2021.03.004

Kothandam, G., Singh, G., Guan, X., Lee, J. M., Ramadass, K., Joseph, S., Benzigar, M., Karakoti, A., Yi, J., & Kumar, P. (2023). Recent Advances in Carbon-Based Electrodes for Energy Storage and Conversion. *Advanced Science, 10*(18), 2301045. https://doi.org/10.1002/advs.202301045

Li, M., Jiang, L., Sun, Y., Xiao, T., Xiang, P., & Tan, X. (2018). Silicon content influence on structure and photoluminescence properties of carbon rich hydrogenated amorphous silicon carbide thin films. *Journal of Alloys and Compounds, 753*, 320-328. https://doi.org/10.1016/j.jallcom.2018.04.226

Mitra, S., Hamada, N., & Mitra, S. K. (2024). Experimental observation and characterization of amorphous carbon generated in graphene on gold nanoparticles. *RSC Advances, 14*(35), 25307-25315. https://doi.org/10.1039/D4RA04893H

Mohagheghpour, E., Rajabi, M., Gholamipour, R., Larijani, M. M., & Sheibani, S. (2016). Correlation study of structural, optical and electrical properties of amorphous carbon thin films prepared by ion beam sputtering deposition technique. *Applied Surface Science, 360*, 52-58. https://doi.org/10.1016/j.apsusc.2015.10.213

Moseenkov, S. I., Kuznetsov, V. L., Zolotarev, N. A., Kolesov, B. A., Prosvirin, I. P., Ishchenko, A. V., & Zavorin, A. V. (2023). Investigation of Amorphous Carbon in Nanostructured Carbon Materials (A Comparative Study by TEM, XPS, Raman Spectroscopy and XRD). *Materials, 16*(3), 1112.

Ono, S., Hwang, S.-H., Okumura, T., Yamashita, N., Kamataki, K., Kiyama, H., Itagaki, N., Koga, K., & Shiratani, M. (2024). Effects of carbon nanoparticle insertion on stress reduction in hydrogenated amorphous carbon films using plasma chemical vapor deposition. *Diamond and Related Materials, 150*, 111654. https://doi.org/10.1016/j.diamond.2024.111654

Orlando, A., Franceschini, F., Muscas, C., Pidkova, S., Bartoli, M., Rovere, M., & Tagliaferro, A. (2021). A comprehensive review on Raman spectroscopy applications. *Chemosensors,* 9(9), 262. https://doi.org/10.3390/chemosensors9090262

Ouyang, D.-d., Hu, L.-b., Wang, G., Dai, B., Yu, F., & Zhang, L.-l. (2021). A review of biomass-derived graphene and graphene-like carbons for electrochemical energy storage and conversion. *New Carbon Materials, 36*(2), 350-372. https://doi.org/10.1016/S1872-5805(21)60024-0

Priyanto, B., Khambali, I., Ardiani, I. S., Nadhiyah, K., Laila, A. Z., Hasani, M. C., Romadhon, B., Asih, R., & Cahyono, Y. (2024). Nitrogen-Doped Amorphous Carbon Homojunction from Palmyra Sugar as a Renewable Solar Cell. *Journal of Renewable Materials, 12*(1). https://doi.org/10.32604/jrm.2023.028619

Robaiah, M., Asli, N. A., Abdul Rani, R., Abdullah, W. F. H., Khusaimi, Z., Azhan, H., Abdullah, S., & Rusop, M. (2023). A PMMA-assisted transfer method of waste cooking palm oil based multi-layered graphene from a nickel substrate onto a glass substrate for the development of a humidity sensor. *Journal of Materials Science: Materials in Electronics, 34*(16), 1287. https://doi.org/10.1007/s10854-023-10591-8

Roy, A., Wang, S., & Komvopoulos, K. (2023). A review of plasma-assisted deposition methods for amorphous carbon thin and ultrathin films with a focus on the cathodic vacuum arc technique. *Journal of Materials Research, 38*(3), 586-616. https://doi.org/10.1557/s43578-022-00868-9

Saputri, D. D., Jan'ah, A. M., & Saraswati, T. E. (2020, October). Synthesis of Carbon Nanotubes (CNT) by Chemical Vapor Deposition (CVD) using a biogas-based carbon precursor: A review. In *IOP Conference Series: Materials Science and Engineering* (Vol. 959, No. 1, p. 012019). IOP Publishing.

Yan, Y., Nashath, F. Z., Chen, S., Manickam, S., Lim, S. S., Zhao, H., Lester, E., Wu, T., & Pang, C. H. (2020). Synthesis of graphene: Potential carbon precursors and approaches. *Nanotechnology Reviews,* 9(1), 1284-1314.

Zhang, C. C., Hartlaub, S., Petrovic, I., & Yilmaz, B. (2022b). Raman Spectroscopy Characterization of Amorphous Coke Generated in Industrial Processes. *ACS Omega, 7*(3), 2565-2570. https://doi.org/10.1021/acsomega.1c03456

Zhang, S., Li, Z., Luo, K., He, J., Gao, Y., Soldatov, A. V., Benavides, V., Shi, K., Nie, A., & Zhang, B. (2022a). Discovery of carbon-based strongest and hardest amorphous material. *National Science Review,* 9(1), nwab140. https://doi.org/10.1093/nsr/nwab140

Zhou, T., Hu, W., Yang, Z., Li, J., & Zeng, X. (2023). Study on nutrients, non-volatile compounds, volatile compounds and antioxidant capacity of oyster mushroom cultivated with corn distillers' grains. *LWT, 183*, 114967. https://doi.org/10.1016/j.lwt.2023.114967